Quantum turbulence of bellows-driven ^{4}He superflow: Steady state

S. Babuin,[1] M. Stammeier,[2,*] E. Varga,[2] M. Rotter,[2] and L. Skrbek[2]
[1]*Institute of Physics ASCR, Na Slovance 2, 182 21 Prague, Czech Republic*
[2]*Faculty of Mathematics and Physics, Charles University, Ke Karlovu 3, 121 16 Prague, Czech Republic*
(Received 8 July 2012; published 11 October 2012)

Quantum turbulence in superfluid ^{4}He is studied by the attenuation of second sound in flow channels of 7-mm and 10-mm side square cross sections, and 115-mm length. The ends of the channels are plugged by sintered silver superleaks to allow a pure superflow (i.e., a net flow of the superfluid component only). Flows are generated by mechanically operating a low temperature bellows assembly, as opposed to the helium fountain pump commonly used for previous superflow turbulence studies. The temperature range is $1.35\ \mathrm{K} \leqslant T \leqslant 1.95\ \mathrm{K}$, at the saturated vapor pressure. The observed turbulent steady state is characterized by the vortex line density $L^{1/2} = \gamma(T)(v - v_c)$, where v is the mean superflow velocity and v_c is the critical velocity for the onset of turbulence. The character of the steady state agrees with the Vinen phenomenological model for thermal counterflow turbulence. The coefficient $\gamma(T)$ is in fair agreement with previous thermal pure superflow and counterflow experiments. The critical velocity $v_c \approx 0.2$ cm/s is roughly temperature independent.

DOI: 10.1103/PhysRevB.86.134515 PACS number(s): 67.25.dg, 67.25.dk, 67.25.dm

I. INTRODUCTION

Quantum turbulence (QT)[1] is the most general form of motion of quantum fluids displaying superfluidity, and represents an interesting physical system for a deeper understanding of turbulence in classical fluids, too. QT in superfluid ^{4}He at finite temperature is physically richer than conventional turbulence in viscous fluids because of the two-fluid nature of superfluid helium.[2] The zero-entropy superfluid component can flow without dissipation at low velocity, while being subject to quantum mechanical constraints: The only form of rotational motion allowed is a thin vortex line, whose circulation around the core is not arbitrary as in classical fluids, but quantized in units of $\kappa = 0.997 \times 10^{-7}\ \mathrm{m}^2/\mathrm{s}$.

Unlike the $T \to 0$ K limit where the normal component is absent, at finite temperatures, say for $T \gtrsim 1$ K, QT in superfluid ^{4}He involves the dynamics of a tangle of such quantized vortices coupled by the mutual friction force to the viscous normal fluid component, that itself can easily become turbulent.[3] QT in superfluid ^{4}He at finite temperature thus represents the experimentally easily accessible but intellectually most challenging case. Experimental investigation is instrumental here, as at present neither purely theoretical nor numerical studies are capable of taking into account with sufficient precision all details of mutually interacting turbulent superfluid and normal velocity fields.

In most early works, starting with the pioneering experiments of Vinen,[4] QT was studied in counterflow, the thermally activated motion of normal and superfluid components in opposite directions. Thermal counterflow has a turbulent steady state (in fact, three different turbulent states have been identified by Tough;[5] see later) with no obvious classical counterpart, but displays a classical-like character of its late time decay.[6–9]

When instead QT is generated with methods used for classical flows (resulting in so-called co-flows), similarities with classical turbulence appear more clearly, both in the steady-state properties (Kolmogorov inertial range in energy spectrum in various flows, e.g., between counter-rotating propellers,[10] grid and wake flows in pressurized wind tunnel and "chunk" turbulence flow;[11] Kolmogorov "4/5-law" in pipe flow[12]) as well as in the character of the decay (towed grid,[6,13,14] spin down[15]), despite quantum-mechanical restrictions on the motion of the superfluid component. Experimental research proceeded hand in hand with theoretical and computational studies, starting from the influential work of Schwarz.[16] Comprehensive consideration of theoretical and computational aspects lays beyond the scope of our article, however, two theoretical works closely related to the present project will be discussed in due course.

In general, three distinct cases of ^{4}He QT at $T \gtrsim 1$ K are of particular interest: (i) thermal counterflow, (ii) co-flowing normal and superfluid components, and (iii) pure superflow (i.e., the net flow of the superfluid component only). In this project we have studied properties of QT in pure superflow, generated for the first time mechanically, as opposed to thermally by helium fountain pump, as reported in previous works.[17–19] Low temperature bellows for the generation of superfluid helium pipe flows have been already used by Van Sciver and co-workers who studied pressure drop for steady forced co-flow.[20]

Our project focuses on the single component net flow, integrating measurements of vortex line density by second sound attenuation, in steady and decaying turbulence. Let us stress that, despite that this flow is generated by classical means (mechanical bellows compression), thanks to the ability of superleaks to filter out the normal fluid flow, the resulting steady net pure superflow inside the channel does not have any obvious classical analog. In this article we discuss the steady state and onset of such turbulent flow, while a forthcoming article will be dedicated to its decay. The article is organized as follows: Sec. II describes our experimental setup and protocol, Sec. III contains our experimental results, which are discussed and compared with relevant previous experiments in Sec. IV; we conclude in Sec. V. A step-by-step derivation of the relationship between the vortex line density and the measured amplitude of second sound [which is essential in this work; Eq. (2)], is given in the appendix.

II. APPARATUS AND METHOD

A. Flow channel, flow generation, and thermometry

The apparatus used is illustrated in Fig. 1. A net flow of superfluid component through a flow channel is generated by compressing a stainless steel bellows filled with superfluid ^{4}He and immersed in the open cryostat bath.

Two brass flow channels have been used, with internal square cross section of side 7 mm and 10 mm, and finely polished walls. Both channels are 115-mm long and have an outer dimension of 32 mm. The channel ends are plugged by silver-sintered superleaks (i.e., filters constituted by packing of silver spheres with a 1/2 volume filling fraction), resulting in submicron-sized pores to prevent a net flow of the viscous normal component through the channel on any flow time scale relevant to the experiment.[21] The superleaks are designed having in mind not to plug the internal cross section directly: The channel ends have a roughly conical expansion of diameter 16 mm (not shown in Fig. 1) to which the 2-mm-thick sintered silver superleaks are sintered *in situ*, thus the effective output cross section for the flow through the superleaks is not smaller than the cross section seen by the flow in the channel.

The bellows is driven by a computer-controlled motor located on the cryostat flange at room temperature, and connected to the bellows via gear box and shaft. The motor can perform micron-accuracy positioning and can control the velocity to within about 1%. The mean channel superflow velocity v is calculated by requiring that the mass flow rate of liquid out of the bellows equals the mass flow rate into the channel, assuming the liquid incompressible. The bellows volume has been calibrated at room temperature to within about 2% accuracy. The mean flow velocity in the channel is given by

$$v = v' \frac{\partial V}{\partial h} \frac{1}{A}, \tag{1}$$

where v' is the velocity of the shaft along the vertical displacement h (measured by the motor's encoder), V is the bellows volume, and A is the cross section of the flow channel. The maximum volume that can be displaced by the bellows is about 400 ml, and from the calibration we obtained $\partial V/\partial h = 4.25 \pm 0.08$ ml/mm; overall the flow velocity is known to within 3% accuracy. During cool-down, the bellows is filled with helium gas; liquid helium enters it below the lambda transition via the channel, and it easily fills the whole volume. Flows are studied only when generated by compressing the bellows, not expanding it, that is to say, when the flow velocity can be deduced unambiguously from Eq. (1).[22] Once the bellows is fully compressed, liquid helium is recharged by expanding it.

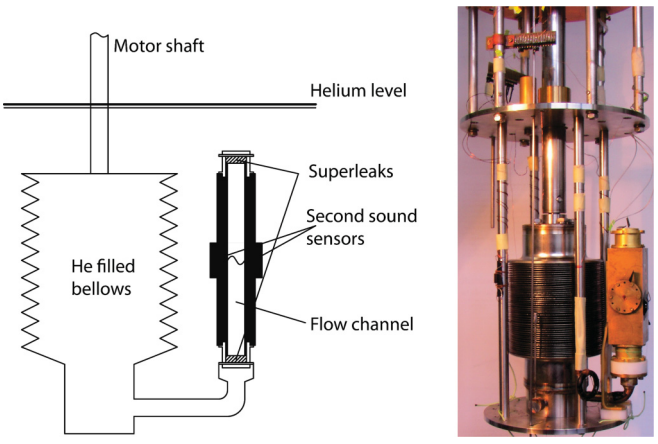

FIG. 1. (Color online) Schematic diagram and photograph of the bellows with the flow channel.

The experiments have been carried out in the temperature range $1.35\ \text{K} \leqslant T \leqslant 1.95\ \text{K}$, at the saturated vapor pressure. The absolute temperature of the bath is deduced from the vapor pressure (measured via a separate line ending in the cryostat close above the liquid bath level) and its fluctuations are measured with a carbon resistance thermometer immersed in the bath near the channel, itself calibrated against the vapor pressure. The bath temperature is controlled either by manual regulation of the pumping rate, or with a temperature controller which uses as a reference the carbon thermometer and a manganin heater wire immersed in the bath. We choose whichever method gives a temperature control of about 1 mK or better. Other two calibrated carbon thermometers are located inside the bellows. All carbon thermometers are used primarily as relative thermometers, since they are slightly affected by thermal cycling. Their absolute reading is accurate to within about 10 mK. No thermometers are installed inside the channel to avoid disturbing the flow.

B. Second sound attenuation

QT is detected by the attenuation of second sound propagating in a direction perpendicular to the mean superflow. The second sound experiences attenuation additional to bulk viscous losses when the thermal excitations constituting the normal component are scattered by the vortex filaments. The second sound speaker and receiver are circular membranes of 9-mm diameter with micron-size holes, located at mid channel length (see Fig. 1; additionally, a blow-up drawing of the channel and more construction details are given in Ref. 19). The speaker membrane induces a second sound wave by oscillating and displacing only the viscous normal component of helium, thereby causing higher local concentration of normal component and hence higher temperature. The channel walls constitute a resonator for such wave. The membranes have one gold-plated side in contact with the channel body biased typically with 100 V and a circular brass electrode is spring loaded against the other side, thus forming a capacitor with one vibrating plate. In order to achieve the highest signal-to-noise ratio, the drive amplitude is adjusted close below the level at which the second sound signal versus drive dependence starts to deviate from linearity—typically between 6 and 10 V.

An example of the signal detected by the second sound receiver is shown in Fig. 2. The figure shows how the resonant curve for quiescent helium is attenuated and broadened as flows of increasing steady-state velocity are produced in the channel. The frequency spectra have been acquired in conditions of fully developed steady flow. Note the existence of additional smaller peaks that most likely occur due to weak coupling to longitudinal second sound resonances in the channel. Experimentally, we always tried to use the harmonics

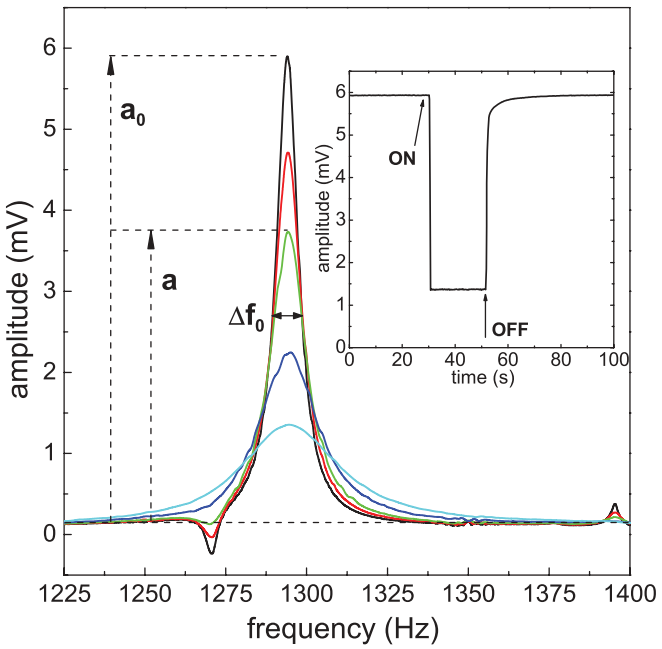

FIG. 2. (Color online) Second sound resonance curves (first mode) for different steady-state flow velocities in the 7-mm wide channel at $T = 1.35$ K. The tallest curve corresponds to the case of no flow in the channel, while others correspond to flow velocities of, from top to bottom, 1.73, 2.60, 4.33, and 6.07 cm/s. (Inset) The second sound amplitude at resonance monitored in time as a flow of steady velocity 6.07 cm/s is switched on and off (same flow velocity as most attenuated curve in main plot).

(in most cases the fundamental or its first overtone) which for particular conditions were least affected by these parasitic resonances. We have, however, thoroughly verified that results are in no way affected by the choice of harmonic.

One can see in Fig. 2 that the central frequency is not changed by the flow. This enables one to carry out a simplified experiment where one samples in time the second sound amplitude *at* the resonant frequency, observing the changes occurring upon switching on a flow, maintaining its steady state, and switching it off. An example of one such time series is shown in the inset and provides the basis for the study of the decay transient.

In this article we shall be solely concerned with the steady-state properties of the flow. The decay transient also contains valuable physical information and will be discussed in a follow-up article. In the steady state the signal is sampled at a rate of 5 points per second, and each point is averaged with a lock-in amplifier time constant of 100 ms (for comparison, the time for a second sound wave traveling at $\approx$20 m/s to complete a return trip in the 1-cm wide channel is 1 ms). The amplitude averaged during the steady state has a standard deviation of less than 1% and during that process the temperature is usually kept constant to better than 1 mK.

The second sound attenuation technique does not detect the absolute vortex line length, but a quantity proportional to the average of the square of the sine of the angle between the vortex lines and the second sound propagation direction.[23] Therefore, to infer the absolute length one needs to know the actual spatial distribution of the lines. This is in general not known, and perhaps cannot be known with certainty unless directly visualized, which is not possible in this setup. Therefore an assumption on the vortex line distribution is necessary. Assuming that the vortex tangle is homogeneous and isotropic, the total length of vortex lines per unit volume L can be deduced from the measurement of the second sound amplitude a as follows:

$$L = \frac{6\pi \Delta f_0}{B\kappa}\left(\frac{a_0}{a} - 1\right), \tag{2}$$

where a_0 and Δf_0 are the amplitude and the full width at half maximum of the second sound resonance without flow, and B is the mutual friction coefficient (tabulated in Ref. 24). All vortex line density computed in this article originates from this equation. Another limiting case exists, that of vortex lines all lying in planes parallel with the direction of second sound propagation, and randomly oriented within that plane. In that case L in Eq. (2) is reduced by a factor 4/3. Hints on the derivation of this equation are provided, for example, in Refs. 25 and 9 but a full derivation is given here for convenience in the appendix. The non-attenuated resonance width Δf_0 is obtained from a Lorentzian fit of the full resonant curve as shown in Fig. 2, while a_0 and a have been obtained both from fits and from averaging the amplitude signal of the type shown in the inset.

C. Temperature gradients

In this final section we turn to a discussion of the distribution of temperature in the system. During steady flow the helium *inside the bellows* becomes warmer (as measured by local thermometers), due to the reduction of the superfluid component fraction. Such increase is roughly linear with flow velocity, and roughly independent of mean temperature; it is at most 3 mK for the highest flow velocities considered in this article, of about 20 cm/s. The temperature in the bath, instead, is almost unchanged.

It is important to realize that the warming up of helium inside the bellows cannot alter the mass flow rate through the channel—which is entirely set by the rate of bellows compression—therefore it does not affect the determination of v discussed before. The helium in the channel is in fact thermally well separated from both the helium in the bellows and in the bath, because of low thermal conductivity of brass walls and silver sinter.[26]

Regarding the temperature gradient in the helium *inside the channel*, since no local thermometers are present, an estimation is possible from the two-fluid equations of motion. Subtracting the superfluid from the normal fluid momentum conservation equations in the steady state [see Eqs. (A3) and (A4) in the appendix], and neglecting nonlinear terms and viscous dissipation, one can show that a thermal gradient $\nabla T = \mathbf{F}_{ns}/(\rho_s \sigma)$ arises to balance the mutual friction force $\mathbf{F}_{ns}$, where ρ_s is the density of the superfluid component and σ is the entropy of helium per unit mass. For a tangle of randomly oriented vortex lines we estimate $\nabla T \approx -\kappa \rho_n B L(\mathbf{v}_n - \mathbf{v}_s)/(3\rho\sigma)$, where for $\mathbf{F}_{ns}$ we have used Eqs. (A6) and (A18), $\mathbf{v}_n$ and $\mathbf{v}_n$ are the normal and superfluid velocities, and ρ and ρ_n are, respectively, the total density of helium and of the normal component. For our channel, assuming the normal fluid is at

rest ($\mathbf{v}_n = 0$), we arrive at a maximal temperature difference of order 10 mK for the highest attainable flow velocities, with the temperature increasing along the direction of the superflow. Note incidentally that such thermal gradient exists irrespectively of whether the superflow is driven mechanically (by a bellows) or thermally (by a fountain pump, as in Ref. 19), and has the same orientation.

III. RESULTS

A. Vortex line density versus mean velocity

The steady-state vortex line density is plotted as $L^{1/2}$ versus the mean superflow velocity v in Fig. 3, for the 7-mm-wide channel. Symbols distinguish values of L obtained from the second sound amplitude a, extracted from a Lorentzian fit of the full resonant curve (open symbols), from those for which a is measured directly at resonance (solid symbols), as described in Sec. II B. This second approach is required for $v \gtrsim 10$ cm/s, when the time for the bellows to complete a compression becomes shorter than the time required for a sufficiently detailed scan of the resonance; both approaches agree very well. The data sets are fitted with straight lines of the form,

$$L^{1/2} = \gamma(T)(v - v_c), \tag{3}$$

and the fit is weighted against the relative importance of the experimental error on L. The inset shows that the fitted lines extrapolate to a nearly temperature independent intercept $v_c \approx 0.1$ cm/s. This form of $L(v)$ agrees with the steady-state solution of Vinen's phenomenological equation,[4] which describes well steady-state counterflow.

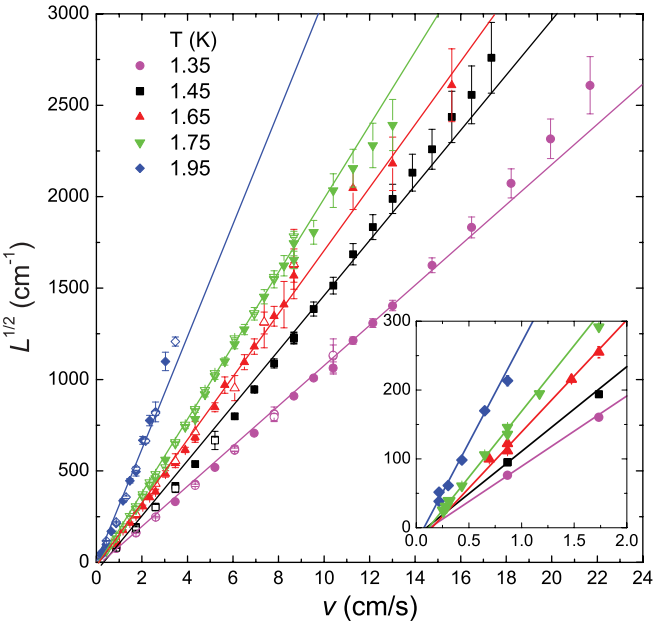

FIG. 3. (Color online) The square root of the steady-state vortex line density L, as a function of mean superflow velocity v, for the 7-mm wide channel, at different temperatures. Open symbols relate to L obtained from the second sound amplitude a extracted from a Lorentzian fit of the full resonant curve, while solid symbols relate to a directly measured at resonance. Straight lines are fits to the data weighted by the uncertainty in L. The inset highlights the existence of a positive intercept, v_c.

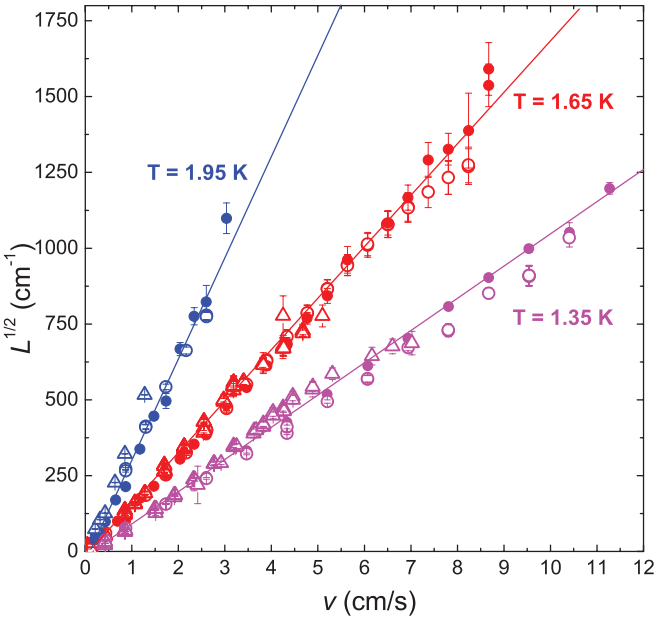

FIG. 4. (Color online) Comparison of results from three different channel configurations. (i) Solid circles, 7-mm channel with both superleaks (as in Fig. 3); (ii) open circles, 7-mm channel with downstream superleak removed; (iii) open triangles, 10-mm channel with both superleaks. Straight lines guide the eye.

In Fig. 4 we show a comparison of some of the data just presented, with results from runs where the downstream superleak was removed from the 7-mm channel and runs with the 10-mm channel with both superleaks present. We see that removal of the downstream superleak does not lead to any appreciable change in the observed steady-state vortex line density in the 7-mm channel, suggesting that the flow is of the same character. Additionally, we find that the observed steady-state vortex line densities in the 7-mm and in the 10-mm channels agree within experimental scatter, again in agreement with Vinen's phenomenological equation.[4]

B. $\gamma(T)$ coefficients

The $\gamma(T)$ coefficients of Eq. (3) are plotted as a function of temperature in Fig. 5, for a variety of systems. Let us first describe the results of the present work. The five slopes of Fig. 3, relating to the 7-mm-wide channel, are represented as solid blue circles, while the green solid squares relate to the same channel with the downstream superleak removed, leading to no appreciable change in γ. The open up-pointing blue triangles are from the 10-mm-wide channel, showing marginally but systematically higher γ than the 7-mm channel. Whether this is attributable to a size effect cannot be easily concluded since, first, only two channel sizes are available, and secondly, the performance of the second sound sensors was poorer in the 10-mm channel run, leading to lower accuracy.

Let us now turn to a comparison with related previous works, starting with two pure superflow experiments. The closest comparison is, in principle, with a previous experiment run in Prague by Chagovets and Skrbek,[19] where the same flow channels and detection technique were used, but the superflow was generated by helium fountain pump, instead of

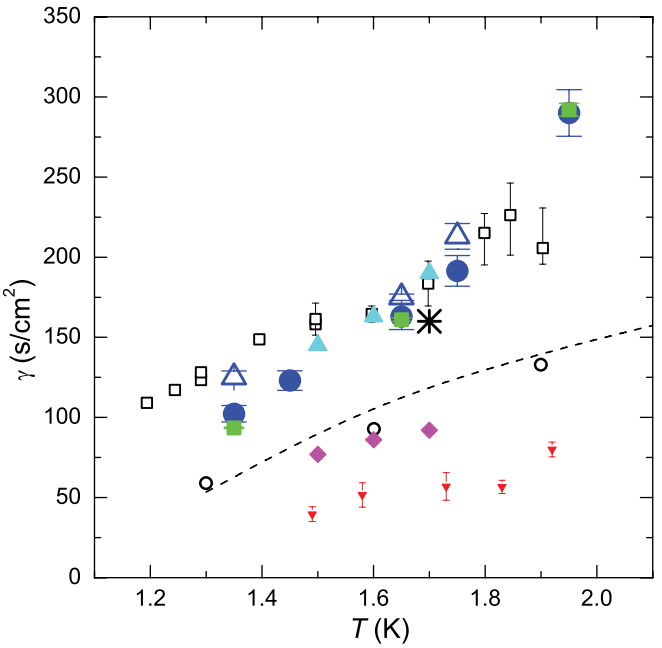

FIG. 5. (Color online) The quantity $\gamma(T)$ of Eq. (3) calculated for available pure superflow and counterflow experiments and simulations. Present work: solid blue circles, 7-mm channel; solid green squares, 7-mm channel, downstream superleak removed; open blue up-triangle, 10-mm channel. Other works: (i) thermally induced pure superflow, open squares, Ashton *et al.*, 0.13-mm diameter glass channel;[17] solid red down-triangle, Chagovets and Skrbek, 7-mm channel as present work, A-state turbulence;[19] (ii) counterflow, solid blue up-triangle, solid magenta diamond, Martin and Tough, TII and TI states, 1-mm diameter glass channel;[27] open circles, Childers and Tough, TI state, 0.13-mm diameter glass channels;[28] asterisk, TII state, 7-mm channel as present work, unpublished; dashed line, *Adachi et al.*, numerical simulation.[29]

bellows. For low velocities (there defined as the A state of pure superflow turbulence) the authors found $L^{1/2} = \gamma(T)(v - v_c)$, while at higher velocities they reported a transition to a B state with $L \propto v$. The A-state slopes are shown here as full down-pointing red triangles: They are very different from the bellows version of the experiment, and also significantly lower than any other surveyed work. As it will be outlined in more detail in Sec. IV, we have now evidence that the flow velocity in the fountain experiment was overestimated by a factor roughly between 2 and 4, depending on temperature and heat current: If corrected by this factor, γ from the fountain-driven flow would be roughly in agreement with the bellows-driven flow. Therefore, for the time being, we shall not be concerned with these results.

We offer instead as relevant comparison the results by Ashton *et al.*,[17] where pure superflow was driven by fountain pump in a cylindrical glass channel, 0.13 mm in diameter, shown as black open squares, in fair agreement with the present work, despite L was deduced from measurements of temperature difference along the channel. Although their channel was very narrow, the average intervortex distance, $1/\sqrt{L}$, was becoming comparable with the channel size only at very low velocity, suggesting that finite size effects did not play an important role, and therefore justifying a comparison with our system.

Let us now consider thermal counterflow experiments. The asterisk marks an unpublished datapoint obtained in Prague with the same 7-mm-wide channel used in this work, but in thermal counterflow. The up-pointing full cyan triangles and the magenta diamonds are from Martin and Tough[27] in a 1-mm-diameter glass channel, relating, respectively, to the TII and TI state of counterflow turbulence. As a reminder, thermal counterflow turbulence in channels with a cross-sectional aspect ratio close or equal to unity and absolute width of order 1 mm or less has been classified by Tough as possessing two turbulent regimes,[5] TI, which immediately follows the laminar state, and TII, occurring above a critical line density, both satisfying $L^{1/2} = \gamma(T)(v - v_c)$ with γ in TII state considerably larger than in TI. These two regimes are not a universal property of counterflow turbulence: A single state has been observed in channels with a very large cross-sectional aspect ratio (although small absolute dimensions, below 1 mm), termed TIII[5] and also in the seminal work of Vinen in channels with cross-sectional aspect ratio of order 1/2, with absolute dimensions of several mm.[4]

In pure superflows only a single regime has ever been observed—the existence of A and B states reported by Chagovets and Skrbek is presently under scrutiny on account of uncertainties on flow velocities occurring in that experiment, as further discussed in Sec. IV B.

The TII state measured by Martin and Tough[27] agrees well with the pure superflow experiments; their corresponding TI state agrees with the TI state in a channel of about 10 times smaller diameter (Childers and Tough, black open circles[28]) and with the numerical simulation of Adachi *et al.*[29] (dashed line). This numerical simulation is based on the solution of the full Biot-Savart integral[23] and therefore takes into account long-range interactions between vortices, and is solved in a domain with periodic boundary conditions. Due to current limitations in computational power, the simulation can reach only modest vortex line densities, within the TI regime.

C. Critical velocities

In the present work we have investigated the critical velocity that corresponds to the onset of QT, by producing long-lasting steady flows (several tens of seconds), gradually increasing the velocity from zero up to a value well into the turbulent regime, and from there reducing it back to zero, observing changes in the second sound amplitude tracked at resonance. An example of such raw data is provided in Fig. 6, where the second sound amplitude is plotted as function of time while the flow velocity is increased in steps of 0.05 cm/s, lasting 50 s each. In this particular case the first departure from noise occurs at around $t = 180$ s, when $v = 0.16$ cm/s. The temperature stability in the bath was 0.1 mK.

Figure 7 shows the mean critical velocity for different systems. Regarding the present work, the ramp-up, and ramp-down critical velocities, averaged over several measurements, are plotted as black open circles and blue open squares, respectively, for the 7-mm channel and as stars for the 10-mm channel (average of very similar ramp-up and ramp-down measurements). These measurements show, within the available resolution, no temperature dependence and no hysteresis effects.

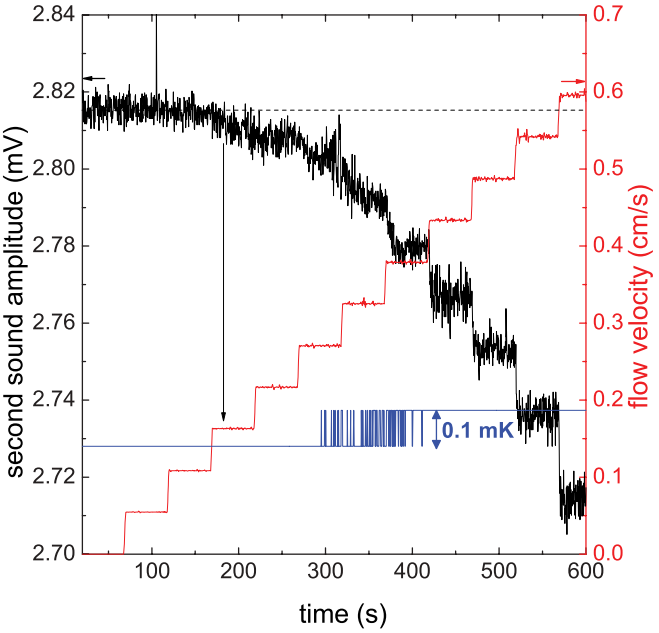

FIG. 6. (Color online) Example of raw data for the determination of critical velocity. The second sound amplitude is tracked at resonance, while the flow velocity is suddenly increased with 0.05 cm/s resolution steps lasting 50 s. Here a change in attenuation distinguishable from the noise floor (dashed line) first appears at around 180 s, when $v = 0.16$ cm/s. The blue line shows the temperature of the bath, stable to within 0.1 mK.

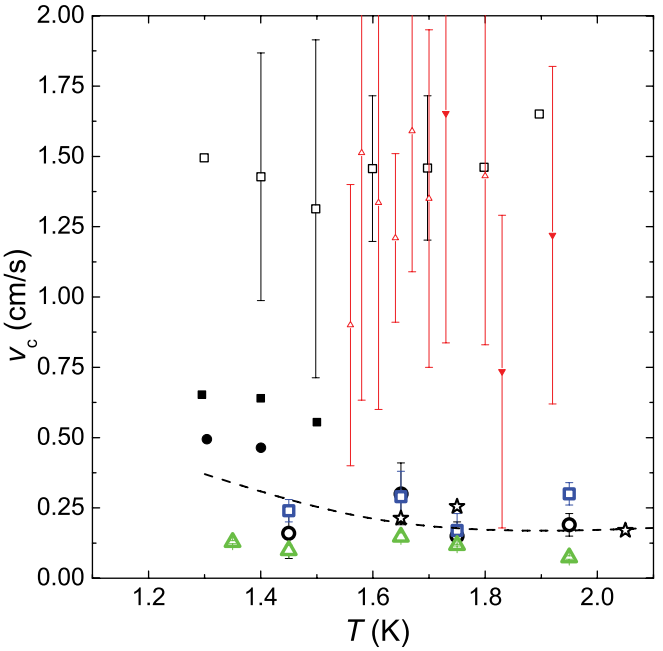

FIG. 7. (Color online) The critical velocity for the onset of turbulence from different experiments and simulations. Present work: open black circles, open blue squares, open green up-triangles = ramp-up, ramp-down, fit extrapolation, 7-mm channel; stars = average of ramp-up and ramp-down, 10-mm channel. Other works: (i) thermal pure superflow, open black squares = Baehr *et al.*, 0.13-mm glass channel;[18] solid red down-triangles = Chagovets and Skrbek, 7-mm and 10-mm channels as in present work;[19] solid black squares, solid black circles = Vinen, 2.4×6.5 mm^2 and 4×7.8 mm^2 channels;[4] dashed line = Adachi *et al.*, numerical simulation.[29]

The results also do not depend on whether the flow velocity is increased (or decreased) quasi-continuously as opposed to in discrete steps, nor do they depend on whether or not the flow velocity is reduced to zero in between each increment in velocity. The averages of ramp-up and ramp-down critical velocities at different temperatures for the 7-mm channel are, respectively, 0.20 ± 0.07 cm/s and 0.25 ± 0.06 cm/s, while the average in the 10-mm channel in 0.21 ± 0.05 cm/s, all agreeing within the uncertainty. For these low flow velocities, the extent of second sound attenuation becomes comparable to the signal noise, as shown in Fig. 6, therefore we conclude that the real critical velocity must be at least as measured, or lower.

The critical velocity can also be estimated from the intersection with the x axis of the straight line fits of Fig. 3 (inset), although this method assumes that the same slope continues to hold at very low velocities. For the 7-mm channel this intercept is 0.11 ± 0.03 cm/s: similar, but a little lower than the direct measurement; this is consistent with the situation in thermal counterflow as summarized by Tough.[5]

Critical velocities found in thermally generated superflow experiments are also provided in Fig. 7. The black open squares are from Baehr *et al.* who used a 0.13-mm diameter glass channel,[18] the same which yielded the black open squares data in Fig. 5, but here the difference with the present work is substantial. Whether or not this counts as a disagreement will depend on whether the critical velocity is an intrinsic property of the flow or depends on channel geometry. Evidence discussed in the next section suggests that the latter is the case.

The red triangles are the critical velocities in the 7-mm and 10-mm-wide channels as used in the present work, but with the fountain-driven superflow.[19] As discussed above, these points are very likely to be incorrect because of the overestimation of superflow velocity, and should for the present purposes be disregarded. If, however, the same temperature-independent correction—which makes the γ coefficients agree—is applied here, we would arrive at a value (temperature-averaged, on account of the large error bars) of 0.50 ± 0.22 cm/s for the thermally induced critical velocity in the 7-mm channel: higher, but consistent with the present bellows experiment which, incidentally, allows for much better control of very low velocities than the fountain method.

The pioneering work of Vinen[4] is also included, with the 2.4×6.5 mm^2 and 4×7.8 mm^2 channels, respectively, in solid black squares and circles.

The simulation of Adachi *et al.*[29] for counterflow with periodic boundary conditions is also shown.

IV. DISCUSSION

A. Pure superflow in the framework of Vinen's counterflow model

The steady-state properties of pure superflow have been analyzed in the previous section according to Eq. (3), in agreement with the steady-state solution of Vinen's model for counterflow.[4] In this model the key parameter which governs the dynamical state of the flow is the counterflow velocity $(\mathbf{v}_n - \mathbf{v}_s)$—no boundary effects are taken into account. The

question now arises as to whether such counterflow framework is sufficient to describe the physics of pure superflow, in other words whether pure superflow can be regarded merely as counterflow in the frame of reference of the normal component ($\mathbf{v}_n = 0$).

From our analysis we conclude that the steady-state solution of the Vinen model gives an equally good *formal* account of both pure superflow and counterflow, and that, further, the γ coefficients for pure superflow are in good quantitative agreement with TII counterflow. However, the fact that a TI counterflow state with much lower γ exists in channels with aspect ratio around unity and sufficiently small absolute cross-sectional dimensions, strongly suggests that the finite size of the channel should be, in general, an additional parameter of the problem.

The transition from TI to TII state has been suggested to be triggered by the transition to turbulence in the normal component,[30] and more recently a convincing experimental evidence that the normal component indeed becomes turbulent for sufficiently high heat currents has been given.[3] What is still missing is a detailed explanation of how the channel cross-section dimensions and shape could control such transition.

What is already well established is that if the channel aspect ratio is sufficiently large, only one regime of counterflow turbulence is observed (TIII, perhaps meaning that the normal component becomes turbulent near or before the onset of turbulence in the superfluid component), and for such regime the γ coefficients are very similar to those of pure superflow. To conclude unequivocally though that counterflow and pure superflow are entirely equivalent, is still a contentious issue, since, for example, the properties of the temporal decay of turbulence are different, especially in the early stages of the decay. This open issue will be explored in a future dedicated article.

Regarding the critical velocity for the onset of turbulence, if the points from Chagovets and Skrbek[19] in Fig. 7 are disregarded on account of their very likely overestimation, it is apparent that the critical velocity decreases in some fashion with increasing channel cross section, a fact which has been long known. The critical velocity for pure superflows and counterflows has been measured in a variety of systems during the decades, and several attempts have also been made to account theoretically for its scaling with channel geometry, which, according to the 1982 review by Tough[5] did not lead to a conclusive theoretical understanding of the problem.

A new theory, however, has recently been proposed by Kruglov,[31] based on the interaction of roton excitations with the walls of the channel. Some results from this work, together with a (partial) survey of experimental data are presented in Fig. 8. The critical velocity v_c is plotted as a function of the smallest dimension of channel cross sections, d. We distinguish pure superflow experiments (solid symbols) from counterflow experiments (open symbols).

Regarding pure superflows, a large compilation of classic results was provided almost half a century ago by Van Alphen *et al.*,[39] from which we have extracted a few, for $d > 10^{-3}$ mm, and present them here (error bars are not provided in the source article); these pure superflow results are temperature independent. We also show the pure superflow data from the 0.13-mm diameter channel of Baehr *et al.*[18] (already shown in Fig. 7, and here temperature averaged) and the two values for our

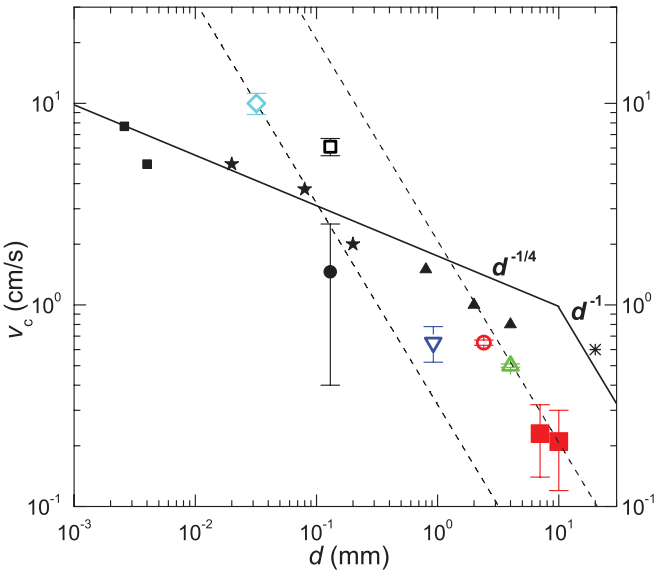

FIG. 8. (Color online) The critical velocity v_c for the onset of turbulence as a function of the smallest dimension of channel cross section d for different systems. Pure superflow experiments (solid symbols), black squares = Hammel & Keller, isothermal flow;[32] stars = Van Alphen *et al.*, adiabatic flow rate;[33] circle = Baehr *et al.*, temperature average of data in Fig. 7;[18] up-triangles = Chase, heat conduction;[34] asterisk = Craig and Pellam, superfluid wind tunnel;[35] red squares = 7×7 mm^2 and 10×10 mm^2, present work, temperature averaged and ramp-up and ramp-down averaged. Counterflow experiments (open symbols), open blue diamond = Ladner and Tough, 0.032×0.32 mm^2;[36] black open square = Childers and Tough, 0.13-mm diameter;[37] blue down-triangle = Yarmchuk and Glaberson, 0.92×11.3 mm^2;[38] open red circle, open green up-triangle = Vinen, 2.4×6.5 mm^2 and 4×7.8 mm^2.[4] Kruglov theory,[31] solid line = predicted absolute scaling of pure superflow critical velocity; dashed lines = predicted scaling for counterflow critical velocity (with undetermined prefactor); lines give a lower and upper bound for the experimental data.

7- and 10-mm channels, also averaged over temperature and ramp-up/ramp-down directions, since we have observed that the critical velocity is almost independent of these parameters. For completeness, we have also added experimental points from some counterflow experiments, for which generally the critical velocity does change with temperature. Here we have chosen values relating to temperatures roughly between 1.3 and 1.35 K, where comparison between different experiments was possible.

The tendency of the critical velocity to decrease with increasing channel size is confirmed, and, although the data points are somehow scattered, it is possible to distinguish different trends for pure superflows and for counterflows. The main part of Kruglov's theory is developed for the case of ideal pure superflows, where the normal component is fully immobilized. The theory predicts $v_c = \Lambda d^{-1/4}$ and $v_c = \Lambda' d^{-1}$, respectively, for $d < 10$ mm and $d > 10$ mm, where Λ and Λ' are calculated theoretical prefactors. This prediction is shown as a solid line. We see that the scaling agrees quite nicely with most pure superflow experimental data, except for the two data points from the present work, which lie about a factor of 5 lower than the prediction.

Van Alphen *et al.*[39] show that in experiments where the normal component is *not* firmly immobilized, a lower critical velocity than predicted by the $d^{-1/4}$ scaling is observed. They argue that in these cases the onset of superfluid turbulence is triggered by a transition to turbulence of the classical type in the normal component, associated with a Reynolds number $\mathrm{Re_n} = v_\mathrm{n} d/\nu_\mathrm{n}$, where ν_n is the effective kinematic viscosity of the normal component. This way, for a given critical $\mathrm{Re_n}$, $v_\mathrm{n} \sim d^{-1}$, and the superfluid critical velocity would scale the same way, from the counterflow conservation of mass condition $\rho_\mathrm{n}\mathbf{v}_\mathrm{n} = -\rho_\mathrm{s}\mathbf{v}_\mathrm{s}$. The authors point out that, conversely, if the normal component is properly immobilized by the use of superleaks, the $d^{-1/4}$ scaling is observed to hold up to rather large channel sizes, as exemplified by the 2-cm wide superfluid wind tunnel used by Craig and Pellam,[35] shown as an asterisk in Fig. 8.

This confirms the view that the turbulence onset is regulated by different physical processes occurring in the normal and superfluid component (classical Reynolds number criterion, versus quantized vortices nucleation) each of which has its own dependence on channel size. Whenever the geometry conditions are such that turbulence onset in the normal component occurs first (at lower velocity) than would occur in the superfluid in its own accord, the transition is triggered in the superfluid, too.

These ideas perhaps suggest that, although our channel is indeed plugged by superleaks, *inside* the channel $\mathbf{v}_\mathrm{n} \neq 0$. This need not imply that there is a net flow of a normal component across the superleaks, merely internal motion of the normal component in the channel. This fact may play a very important role later, in the understanding of the character of turbulence decay.

The Kruglov theory also predicts $v_\mathrm{c} \sim d^{-1}$ scaling for counterflow, where the normal component is free to move, although the prefactor of the scaling is not determined. We have drawn two dashed lines where such prefactor is tuned by a factor of 6.5 in order to enclose all the reported counterflow experimental data. The fact that our two points fall within this band may strengthen the hypothesis that the normal component is not stationary during the observed steady state in the present experiment. This was already suggested by Chagovets and Skrbek[19] about their experiments in Prague performed in identical channels. In the following section we take a closer look at those experiments.

B. Discrepancies between mechanically and thermally driven superflow

In Sec. III we have shown how the present work yielded considerably different $\gamma(T)$ and v_c than its previous realization where the superflow was driven by a heater located inside a nozzle on top of the upper superleak, and held just below the bath surface.[19] In principle one would not expect such a difference to occur solely due to a change in the method of flow generation, because the essential physics of the flow inside the superleak-plugged channel depends on the temperature gradient established along the channel (as argued in Sec. II C) and such gradient would not be conceivably affected by a change of flow source. Therefore we proceed with the assumption that the two turbulent flows ought to have similar properties, and we set out to seek other reasons for the discrepancy.

First, we have carefully re-examined the raw second sound attenuation data from the fountain-driven experiment, and independent evaluation confirms that values of L were determined correctly. We therefore reconsidered the determination of mean superflow velocity. This quantity is unambiguous in the bellows experiment, since it is simply related to the measurement of rate of change of bellows volume. In the fountain experiment, however, the mean superflow velocity was not measured directly, but deduced from the power supplied to the fountain heater placed in the nozzle above the upper superleak $\dot{Q}$ as

$$v = \frac{\dot{Q}}{A\rho_\mathrm{s}\sigma T}. \tag{4}$$

This relationship was shown to be valid under the assumption that $\dot{Q}$ is used *entirely* to drive the flow. However, recent direct measurements in the fountain setup revealed that this is not so, since, for example, a sizeable fraction of the heat provided by the heater is spent to enhance evaporation of liquid helium contained in the nozzle.

We have arranged a few replicas of the original fountain experiment to allow for a direct visual determination of the rate of filling of a calibrated volume downstream the channel, from which we have calculated actual channel velocities. A full account of these measurements, which in themselves for various reasons did not constitute a trivial experiment, will be presented in a dedicated article submitted to the Journal of Low Temperature Physics.

The main message is that Eq. (4) always overestimates the directly measured velocity. In short, for low heat currents v is a few times smaller than predicted (depending on T and $\dot{Q}$) and roughly linear with $\dot{Q}$. This correction brings the γ coefficients of the A state of turbulence of Ref. 19 in rough agreement with those of the bellows-driven flow presented in this article.

An exact correction cannot however be expected, because the flow velocity can be measured - by construction - only while the fluid is filling the calibrated volume, hence before it flows out into the bath, a condition that in principle is different from that of the steady state in Ref. 19. At low heat currents it was also possible, in limited circumstances, to measure second sound attenuation simultaneously. This also confirmed that $L(v)$ of fountain and bellows driven flows are in reasonable agreement. At higher heat currents the measured v grows with $\dot{Q}$ at even slower rate than at low heat currents, and therefore v is even further reduced from the prediction. This suggests that the reported transition from A ($L \propto v^2$) to B ($L \propto v$) states of pure superflow turbulence might be spuriously produced by this effect, hence casting doubts over all conclusions pertaining to steady-state turbulence in Ref. 19.

Precise quantitative conclusions unfortunately cannot be drawn because of the limitations of this direct velocity measurements technique. We stress, however, that the data and discussion of the temporal decay of L in Ref. 19 remains valid, as it is fully independent of knowledge of steady-state flow velocity.

V. CONCLUSIONS

We have presented new measurements of the onset and steady-state turbulence of a net flow of ^{4}He superfluid

component in channels of square cross sections of 7- and 10-mm sides, generated mechanically by a low temperature bellows assembly and detected by the second sound attenuation technique.

The dependence of vortex line density L on mean superflow velocity v from both channels satisfies $L^{1/2} = \gamma(T)(v - v_c)$, and therefore it would seem that this system is formally understood within the framework of Vinen's model for thermal counterflow, which treats superflow as counterflow in the frame of reference of the normal component. The $\gamma(T)$ coefficients indeed agree with previous pure superflows and counterflows in the TII regime (i.e., the regime observed in channels of a large cross section of order unity, and sufficiently high vortex line density). We observed a single turbulence regime across the entire velocity range explored. The onset of turbulence occurs at critical velocities v_c not higher than about 0.2 cm/s, a value that within the experimental resolution is roughly independent of temperature. No hysteresis effects have been observed. However, the critical velocity, when examined in the context of other pure superflow experiments of greatly varying channel width d, is lower than predicted by the law $v_c \sim d^{-1/4}$, which otherwise holds rather generally. This suggests that the normal component, although not flowing past the superleaks, may not be at rest in the channel, therefore triggering turbulence in the superfluid at lower velocities.

This work strengthens what is currently known and understood about fully developed turbulent superfluid channel flows in the temperature range where the interaction between the two velocity fields is important, and also draws attention to the still open and complex problem of transition to turbulence in the two-fluid system. Further characterization of the problem, with more open issues, is provided by the observation of the temporal decay of vortex line density upon suddenly stopping the bellows drive, an aspect which will be discussed in a follow-up article.

ACKNOWLEDGMENTS

The authors greatly acknowledge stimulating discussions with and help from T. V. Chagovets, M. La Mantia, P. Roche, D. Schmoranzer, and W. F. Vinen. This work was supported by Grant No. GAČR 202 08/0276.

APPENDIX: DERIVATION OF AN EXPRESSION TO DEDUCE VORTEX LINE DENSITY FROM SECOND SOUND ATTENUATION

We present here a step-by-step derivation for Eq. (2). The plan is to derive the second sound wave equation from the two-fluid equations of motion; set up the resonant conditions for the flow channel; find an expression for the attenuation by vortex lines of the second sound amplitude; and obtain workable equations for the vortex line density L from assumptions on the spacial distributions of the vortex lines.

Let us start from the set of two-fluid model equations, in the limit of small normal and superfluid velocities $\mathbf{v}_n$ and $\mathbf{v}_s$ and in the presence of the mutual friction force $\mathbf{F}_{ns}$.[23] The following equations are, respectively, the conservation of mass, entropy (σ, per unit mass), and momentum for the superfluid and normal components:

$$\frac{\partial}{\partial t}(\rho_n + \rho_s) = -\nabla \cdot (\rho_n \mathbf{v}_n + \rho_s \mathbf{v}_s), \tag{A1}$$

$$\frac{\partial(\rho\sigma)}{\partial t} = -\nabla \cdot (\rho\sigma \mathbf{v}_n), \tag{A2}$$

$$\rho_s \left(\frac{\partial \mathbf{v}_s}{\partial t} + (\mathbf{v}_s \cdot \nabla)\, \mathbf{v}_s \right) = -\frac{\rho_s}{\rho}\nabla p + \rho_s \sigma \nabla T - \mathbf{F}_{ns}, \tag{A3}$$

$$\rho_n \left(\frac{\partial \mathbf{v}_n}{\partial t} + (\mathbf{v}_n \cdot \nabla)\mathbf{v}_n \right) = -\frac{\rho_n}{\rho}\nabla p - \rho_s \sigma \nabla T + \eta_n \nabla^2 \mathbf{v}_n + \mathbf{F}_{ns}. \tag{A4}$$

Symbols still undefined are the pressure p and the dynamic viscosity of the normal component η_n. The mutual friction force per unit volume is given by[40]

$$\mathbf{F}_{ns} = B\frac{\rho_n \rho_s}{\rho}\hat{\mathbf{\Omega}} \times [\mathbf{\Omega} \times (\mathbf{v}_n - \mathbf{v}_s)] + B'\frac{\rho_n \rho_s}{\rho}\mathbf{\Omega} \times (\mathbf{v}_n - \mathbf{v}_s), \tag{A5}$$

which applies to the case of a cylindrical container of superfluid rotating around the central axis with angular velocity $\mathbf{\Omega}$ (i.e., the case in which the vortex lines are oriented parallel with the axis of rotation). The coefficient B is of order unity; the second nondissipative term in B' is assumed small enough to be neglected.

Since in the uniformly rotating container the full length of vortex lines contributes to the angular velocity (no self-canceling lines oriented in random directions) we can write $\mathbf{L} = 2\mathbf{\Omega}/\kappa$, where the orientation of $\mathbf{L}$ gives the orientation of the lines at a given point. Neglecting the second term, Eq. (A5) reduces to

$$\mathbf{F}_{ns} = -B\kappa\frac{\rho_s \rho_n}{2\rho} L(\mathbf{v}_n - \mathbf{v}_s)\sin^2\theta, \tag{A6}$$

where θ is the angle between $\mathbf{L}$ and $\mathbf{v}_{ns} = \mathbf{v}_n - \mathbf{v}_s$. For the sake of clarity, notice that in this derivation by $\mathbf{v}_{ns}$ we do not mean the main counterflow velocity along the channel direction caused by the bellows, but the counterflow velocity associated with the second sound wave, propagating perpendicular to the channel. The fact that the mutual friction force is proportional to $\sin^2\theta$ is referred to as the "sine squared law".[41]

To proceed, we can neglect the nonlinear terms in velocity on the left-hand side of Eqs. (A3) and (A4) (this is possible because in experiments we work in a regime where the second sound driving amplitude is small enough to prevent generation of turbulence) and we neglect the viscous dissipation in Eq. (A4) (because of the small viscosity of the normal component), then by multiplying Eq. (A3) by ρ_n/ρ_s and subtracting it from Eq. (A4) we obtain

$$\rho_n \frac{\partial \mathbf{v}_{ns}}{\partial t} = -\rho\sigma\nabla T + \frac{\rho}{\rho_s}\mathbf{F}_{ns}. \tag{A7}$$

If we further assume that the counterflow velocity $\mathbf{v}_{ns}$ and derivatives of density and entropy are small, combining Eqs. (A1) and (A2) and neglecting terms nonlinear in small quantities we get

$$\nabla \cdot \mathbf{v}_{ns} = -\frac{\rho}{\sigma\rho_s}\frac{\partial\sigma}{\partial t}. \tag{A8}$$

Now we seek a solution for a second sound traveling wave in the form of small perturbations σ' and T' around constant values of σ_0 and T_0 of entropy and temperature, while leaving pressure and density constant. With these simplifications Eq. (A8) can be written as

$$\nabla \cdot \mathbf{v}_{\rm ns} = -\frac{\rho\sigma}{\rho_{\rm n} c_2^2}\frac{\partial T}{\partial t}, \tag{A9}$$

where

$$c_2 = \sigma\sqrt{\frac{\rho_{\rm s}}{\rho_{\rm n}}\left(\frac{\partial T}{\partial \sigma}\right)_{\rho}} \tag{A10}$$

is the velocity of second sound. Substituting Eq. (A6) to Eq. (A7) and solving for ∇T leads to

$$\nabla T = -\frac{\rho_{\rm n}}{\sigma\rho}\left(\frac{B\kappa L}{2}(\sin^2\theta)\mathbf{v}_{\rm ns} + \frac{\partial \mathbf{v}_{\rm ns}}{\partial t}\right). \tag{A11}$$

Taking the gradient of Eq. (A9) and interchanging time and space derivatives we obtain

$$\nabla(\nabla \cdot \mathbf{v}_{\rm ns}) = \frac{1}{c_2^2}\left(\frac{B\kappa L}{2}(\sin^2\theta)\frac{\partial \mathbf{v}_{\rm ns}}{\partial t} + \frac{\partial^2 \mathbf{v}_{\rm ns}}{\partial t^2}\right). \tag{A12}$$

We now consider a second sound plane wave traveling along the z direction with angular frequency ω and wave vector $k\mathbf{e}_z$.

$$\mathbf{v}_{\rm ns} = \mathbf{e}_z v_{ns0} e^{i(\omega t - kz)}. \tag{A13}$$

Substituting this to Eq. (A12) we obtain

$$k = \pm\frac{\omega}{c_2}\sqrt{1 - i\frac{B\kappa L}{2\omega}\sin^2\theta}. \tag{A14}$$

The vortex line density measured in experiments usually ranges from 10^4 to 10^6 cm^{-2}, making κL of order of 1–100 Hz. The frequency of second sound used in experiments is of order 1 kHz.

We can therefore usually (see later) limit ourselves with the first two terms of Taylor expansion of the square root, and since only the negative sign solution is physically meaningful we obtain

$$k = -\frac{\omega}{c_2}\left(1 - i\frac{B\kappa L}{4\omega}\sin^2\theta\right). \tag{A15}$$

Substituting this back to Eq. (A13) we get the propagation of an attenuated wave,

$$\mathbf{v}_{\rm ns} = \mathbf{e}_z v_{ns0}\exp\left[i\left(\omega t - \frac{\omega}{c_2}z\right) - \alpha z\right], \tag{A16}$$

where the attenuation constant is

$$\alpha = \frac{B\kappa L}{4c_2}\sin^2\theta. \tag{A17}$$

Now we need to replace $\sin^2\theta$ by its mean value, making an assumption on the spatial distribution of vortex lines. Assuming a homogeneous and isotropic distribution, and choosing a coordinate system so that $\mathbf{v}_{\rm ns}$ always lies along the z axis, we get

$$\langle\sin^2\theta\rangle = \frac{1}{4\pi}\int_0^{2\pi}\int_0^{\pi}(\sin^3\theta)d\theta{\rm d}\phi = \frac{2}{3}, \tag{A18}$$

and thus the attenuation constant for randomly oriented vortex lines is

$$\alpha = \frac{B\kappa L}{6c_2}. \tag{A19}$$

Note that if the tangle were completely polarized in the direction perpendicular to the propagation of second sound, the result in Eq. (A18) would be 1/2. So if the assumption of homogeneity and isotropy were wrong, Eq. (A19) would be at worst a factor 4/3 higher than the true value. The attenuation of the second sound amplitude by mutual friction adds to the ordinary bulk viscous attenuation. To account for this, we decompose the attenuation constant to a part independent of flow, and one given by Eq. (A19):

$$\tilde{\alpha} = \alpha_0 + \alpha. \tag{A20}$$

The attenuation constant is related to the quality factor of a resonator $Q = f_0/\Delta f$ where f_0 is the resonance frequency and Δf is full width at half maximum of resonance the curve, through

$$\tilde{\alpha} = \frac{\pi}{\lambda Q} = \frac{\pi\Delta f}{c_2}, \tag{A21}$$

where λ is the resonant wavelength.

When the second sound is excited at resonant frequency the waves reflected at the receiver will constructively interfere with the waves emitted from the transducer, giving the total measured amplitude,

$$a = a_e\sum_{n=1}^{+\infty}e^{-\tilde{\alpha}D} = \frac{a_e}{e^{\tilde{\alpha}D} - 1} \approx \frac{a_e}{\tilde{\alpha}D}, \tag{A22}$$

where D is channel width and a_e is amplitude of the wave excited by the transducer. Using Eqs. (A20) and (A21) we arrive at

$$\alpha = \frac{\pi\Delta f}{c_2}\left(\frac{a_0}{a} - 1\right). \tag{A23}$$

Here a_0 is the amplitude when there is no flow in the channel and a is the amplitude with the flow. Finally, using Eq. (A19) we obtain

$$L = \frac{6\pi\Delta f}{B\kappa}\left(\frac{a_0}{a} - 1\right). \tag{A24}$$

This is the required formula (2) that gives vortex line density as a function of directly measurable quantities.

If further terms in the Taylor expansion of Eq. (A14) are considered one can arrive at the following more exact expression (see also Ref. 9):

$$L' = \frac{3c_2}{B\kappa D}\ln\left(\frac{1 + p^2P + \sqrt{2p^2P + p^4P^2}}{1 + P + \sqrt{2P + P^2}}\right), \tag{A25}$$

where $p = a_0/a$ and $P = 1 - \cos(2\pi D\Delta_0/c_2)$, with $D\Delta_0/c_2$ small. The version of Eq. (A24) becomes an overestimation of the true vortex line density provided by Eq. (A25) at extremely high L. From a practical point of view, there is no need to use L' instead of L as long as $(L - L')/L'$ remains much lower than about 30%, which is the maximum uncertainty in L introduced by not knowing the exact spacial distribution of vortex lines. For our channels with $D = 7$ mm, we find $(L - L')/L' = 30\%$ at $L' \approx 3 \times 10^7$ cm^{-2}. The maximum L reported in this paper is about 8×10^6, for which $(L - L')/L' \cong 8\%$.

*Department of Physics, ETH Zurich, Schafmattstr. 16, CH-8093 Zürich, Switzerland.

[1]W. F. Vinen and J. J. Niemela, J. Low Temp. Phys. **128**, 167 (2002); L. Skrbek and K. R. Sreenivasan, Phys. Fluids **24**, 011301 (2012).

[2]D. R. Tilley and J. Tilley, *Superfluidity and Superconductivity*, 3rd ed. (Institute of Physics Publishing, Bristol and Philadelphia, 1990).

[3]W. Guo, S. B. Cahn, J. A. Nikkel, W. F. Vinen, and D. N. McKinsey, Phys. Rev. Lett. **105**, 045301 (2010).

[4]W. F. Vinen, Proc. R. Soc. **240**, 114 (1957); **240**, 128 (1957); **242**, 493 (1957); **243**, 400 (1958).

[5]J. T. Tough, in *Progress in Low Temperature Physics*, Vol. VIII (North-Holland, Amsterdam, 1982).

[6]M. R. Smith, R. J. Donnelly, N. Goldenfeld, and W. F. Vinen, Phys. Rev. Lett. **71**, 2583 (1993).

[7]L. Skrbek, A. V. Gordeev, and F. Soukup, Phys. Rev. E **67**, 047302 (2003).

[8]A. V. Gordeev, T. V. Chagovets, F. Soukup, and L. Skrbek, J. Low Temp. Phys. **138**, 549 (2005).

[9]C. F. Barenghi and L. Skrbek, J. Low Temp. Phys. **146**, 5 (2007).

[10]J. Maurer and P. Tabeling, Europhys. Lett. **43**, 29 (1998).

[11]J. Salort, B. Baudet, B. Castaing, F. Chabaud, T. Daviaud, P. Didelot, B. Diribarne, Y. Dubrulle, F. Gagne, A. Gauthier, B. Girard, B. Hebral, B. Rousset, P. Thibault, and P. E. Roche, Phys. Fluids **22**, 125102 (2010).

[12]J. Salort, B. Chabaud, E. Leveque, and P. E. Roche, Europhys. Lett. **97**, 34006 (2012).

[13]S. R. Stalp, L. Skrbek, and R. J. Donnelly, Phys. Rev. Lett. **82**, 4831 (1999).

[14]L. Skrbek, J. J. Niemela, and R. J. Donnelly, Phys. Rev. Lett. **85**, 2973 (2000).

[15]P. M. Walmsley, A. I. Golov, H. E. Hall, W. F. Vinen, and A. A. Levchenko, J. Low Temp. Phys. **153**, 127 (2008); P. M. Walmsley and A. I. Golov, Phys. Rev. Lett. **100**, 245301 (2008).

[16]K. W. Schwarz, Phys. Rev. B **18**, 245 (1978); **31**, 5782 (1985); **38**, 2398 (1988).

[17]R. A. Ashton, L. B. Opatowsky, and J. T. Tough, Phys. Rev. Lett. **46**, 658 (1981).

[18]M. L. Baehr, L. B. Opatowsky, and J. T. Tough, Phys. Rev. Lett. **51**, 2295 (1983).

[19]T. V. Chagovets and L. Skrbek, Phys. Rev. Lett. **100**, 215302 (2008); J. Low Temp. Phys. **153**, 162 (2008).

[20]S. Fuzier, B. Baudouy, and S. W. Van Sciver, Cryogenics **41**, 453 (2001).

[21]To test this assumption, we have forced normal liquid helium (above the lambda transition) against the superleak using the maximum force provided by the motor, 320 N, applied on the bellows effective area of 42.5 cm^2, thereby causing an overpressure in the helium of about 75 kPa. The motor encoder did not measure any displacement during tens of minutes, indicating no measurable viscous flow occurred through the superleak.

[22]On expanding the bellows the flow through the channel faithfully follows the bellows motion only up to a limited, rather low, velocity, due to the small (few Torr, depending on the temperature) overpressure of the helium vapor above the liquid helium in the bath.

[23]C. F. Barenghi and Y. A. Sergeev, *Vortices and Turbulence at Very Low Temperature* (Springer, Wien/New York, 2008).

[24]R. J. Donnelly and C. F. Barenghi, J. Phys. Chem. Ref. Data **27**, 1217 (1998).

[25]C. F. Barenghi, A. V. Gordeev, and L. Skrbek, Phys. Rev. E **74**, 026309 (2006).

[26]Heat transport through helium-filled silver-sintered superleaks can occur via conduction through the silver material and via conduction through the normal component (negligible), since the superfluid cannot carry heat and the viscous normal component cannot convect because it is immobilized in the pores. To estimate heat conduction through the silver itself we used the typical electrical resistivity of silver sinters with $\approx 1/2$ volume packing and purity RRR = 10–20, used for dilution refrigerators, $R \approx 10\,\mu\Omega$cm;[42] we applied the Wiedemann-Franz law to convert electrical resistivity into thermal conductivity (due to electrons, neglecting the lattice contribution) $k_c = \mathcal{L}T/R$, where $\mathcal{L} = 2.44 \times 10^{-8}$ WΩK^{-2} is the Lorenz number. We find $k_c \approx 10^{-2}$ Wcm^{-1}K^{-1}. From the Fourier law for heat conduction we arrive at the power transferred across the superleak $\dot{Q} = k_c A \Delta T/d \approx 10^{-4}$ W, for surface area $A \approx 2$ cm^2 and thickness $d = 0.2$ cm, and for the typical excess temperature in the bellows $\Delta T \approx 1$ mK. Note that this calculated heat input would cause a maximum counterflow velocity in the channel $v_{ns} = v_n - v_s = \dot{Q}/(A\rho_s \sigma T) = 3 \times 10^{-3}$ cm/s,[2] where v_n and v_s are the normal and superfluid velocities, ρ_s is the superfluid density, and σ the entropy per unit mass of helium. Such counterflow velocity is negligible compared with any flow velocity relevant to this experiment, hence the finite thermal conductivity of the superleaks is not an important issue. A similar argument rules out thermal losses through brass walls, even smaller than through superleaks.

[27]K. P. Martin and J. T. Tough, Phys. Rev. B **27**, 2788 (1983).

[28]R. K. Childers and J. T. Tough, Phys. Rev. B **13**, 1040 (1976).

[29]H. Adachi, S. Fujiyama, and M. Tsubota, Phys. Rev. B **81**, 104511 (2010).

[30]D. J. Melotte and C. F. Barenghi, Phys. Rev. Lett. **80**, 4181 (1998).

[31]V. I. Kruglov, Phys. Lett. A **375**, 4058 (2011).

[32]E. F. Hammel and W. E. Keller, Cryogenics **5**, 245 (1965).

[33]W. Vermeer, W. M. Van Alphen, J. F. Olijhoek, K. W. Taconis, and R. De Bruyn Ouboter, Phys. Lett. **18**, 265 (1965).

[34]C. E. Chase, Phys. Rev. **127**, 361 (1962).

[35]P. P. Craig and J. R. Pellam, Phys. Rev. **5**, 1109 (1957).

[36]D. R. Ladner and J. T. Tough, Phys. Rev. B **20**, 2690 (1979).

[37]R. K. Childers and J. T. Tough, Phys. Rev. Lett. **31**, 911 (1973).

[38]E. G. Yarmchuk and W. I. Glaberson, J. Low Temp. Phys. **36**, 381 (1979).

[39]W. M. Van Alphen, G. J. Van Haasteren, R. De Bruyn Ouboter, and K. W. Taconis, Phys. Lett. **20**, 474 (1966).

[40]H. E. Hall and W. F. Vinen, Proc. R. Soc. **238**, 204 (1957); **238**, 215 (1957).

[41]H. A. Snyder and Z. Putney, Phys. Rev. **150**, 110 (1966); P. Mathieu, B. Placais, and Y. Simon, Phys. Rev. B **29**, 2489 (1984).

[42]F. Pobell, *Matter and Methods at Low Temperature*, 3rd ed. (Springer, New York, 2007).